RESEARCH ARTICLE

Wideband Low-Profile Eight-Port Eight-Wave Annular-Ring Patch Antenna Based on Using Eight Dual-Shorted Dual-Resonant Ring Sectors for 8 × 8 MIMO Mobile Devices

KIN-LU WONG[1], (Fellow, IEEE), HUI-CHIH KAO[1], (Student Member, IEEE), AND WEI-YU LI[2], (Member, IEEE)
[1]Department of Electrical Engineering, National Sun Yat-sen University, Kaohsiung 80424, Taiwan
[2]Information and Communications Research Laboratories, Industrial Technology Research Institute, Hsinchu 31057, Taiwan

Corresponding author: Kin-Lu Wong (wongkl@mail.nsysu.edu.tw)

ABSTRACT A wideband eight-port eight-wave annular-ring (AR) patch antenna for 8 × 8 MIMO mobile devices is presented. The AR patch antenna is formed into eight dual-resonant 45°-ring sectors to radiate eight very-low-correlated or generally uncorrelated waves for 8 × 8 MIMO application. Each ring sector is loaded with two shorting pins and excited by a simple probe feed to generate its half- and quarter-wavelength resonant modes at close frequencies to form a dual-resonant wide operating band. Additionally, all 16 shorting pins of the eight ring sectors have a same distance to the patch center, thereby forming a shorting circle to function like a circular metal wall in the AR patch. This makes the surface currents coupled from the excited ring sector to adjacent sectors to be mainly confined inside the shorting circle. Therefore, with the eight probe feeds located outside the shorting circle in the AR patch, enhanced port isolation is obtained. With the proposed design, the eight-port AR patch antenna having a low profile of 1.4 mm (about 0.028λ at 5.9 GHz) and an outer diameter of 46 mm (about 0.91λ at 5.9 GHz) can generate eight very-low-correlated waves over a wide band of about 5.9-7.2 GHz (fractional bandwidth 20% based on 3:1 VSWR for mobile device application). Also, the proposed antenna has a back ground plane and is especially suitable for on-metal surface application. The use of a single proposed antenna can be conveniently applied for the mobile device or Internet-of-Things (IoT) device to cover such as 5.925-7.125 GHz for 8 × 8 MIMO operation in the possible new mobile communication spectrum.

INDEX TERMS Mobile antennas, mobile MIMO antennas, multiport single-patch antennas, low-profile wideband eight-port patch antennas, 8 × 8 MIMO antennas.

I. INTRODUCTION

As compared to the current 4 × 4 multi-input-multi-output (MIMO) operation experienced for fifth-generation (5G) communication users, the higher-order (8 × 8) MIMO operation is envisioned to be applied in the mobile device for sixth-generation (6G) communications [1] to support much higher data rates for the users [2]. In addition, new frequency spectrums suitable for the higher-order MIMO communication are required, such as the 6 GHz band (5.925-7.125 GHz) for the possible new spectrum for mobile communication [3], [4] or the unlicensed WiFi-6E operation [5], [6]. For the promising 8 × 8 MIMO operation such as in the 6 GHz band, the required eight MIMO antennas in a compact and wideband structure yet having good antenna performance for the mobile device application, however, is a great design challenge.

Recently, for 5G 4 × 4 MIMO operation of the mobile device, it has been demonstrated that four MIMO antennas in the form of the four-antenna module [7], [8], or four

The associate editor coordinating the review of this manuscript and approving it for publication was Barbara Masini.

conjoined printed slot antennas [9] or four-port single-patch antenna [10], all backed by a ground plane and having a low profile, are expected to find on-metal surface applications for 5G Internet-of-Things (IoT) devices [10], [11] or on the back side of the display panel of the laptop computers [12]. They may also find applications to be applied on the backcover side of the future smartphone or tablet device [7], [8], [9].

The design concept of the compact four-port single-patch antenna has also been applied for 5G 4×4 MIMO access points with a high antenna profile (larger than 0.1 wavelength in the operating band [13], [14], [15], [16], [17]). To apply these four-antenna modules or four-port patch antennas for 8×8 MIMO operation, however, two such four-antenna elements formed into 1×2 array are required. In this case, a certain spacing between two four-antenna elements to achieve acceptable port isolation thereof is needed. This however increases the total size of the 1×2 four-antenna array to provide eight radiating waves for 8×8 MIMO operation.

In order to further achieve higher MIMO antenna density, the six-port single-patch antennas for applications in the mobile device [18] or access point [19], [20] have also been reported very recently. By using such a single six-antenna element, it is still not sufficient to cover the 8×8 MIMO operation.

In this study, a wideband eight-port eight-wave annular-ring (AR) patch antenna as a compact eight-antenna module for the mobile device or IoT device to support 8×8 MIMO operation in the 6 GHz band (5.925-7.125 GHz, the possible new spectrum for mobile communication or the unlicensed WiFi-6E operation [3], [4], [5], [6]) is presented. The proposed eight-port antenna is backed by a ground plane and has a low profile of 1.4 mm (about 0.028λ at 5.9 GHz). Also, the outer diameter of the AR patch is 46 mm only (about 0.91λ at 5.9 GHz). The eight-port patch antennas can generate eight very-low-correlated waves over a wide band of about 5.9-7.2 GHz (fractional bandwidth 20% based on 3:1 VSWR for mobile device application [7], [8], [9], [10]) to cover the 6 GHz band.

The wideband operation for all the eight ports is obtained by using eight dual-shorted dual-resonant 45°-ring sectors formed in the AR patch antenna. Each ring sector is short-circuited to the ground plane through two shorting pins, thereby generating its 0.5- and 0.25-wavelength modes at close frequencies to achieve dual-resonant wideband operation. In addition, all the 16 shorting pins of the eight ring sectors are arranged to form a shorting circle, which functions like a circular metal wall to achieve enhanced port isolation in the eight-port patch antenna.

The eight-port single-patch antenna studied here is believed to be the first multiport single-patch antenna in the open literature to support eight very-low-correlated or generally uncorrelated waves for on-metal surface applications. For comparison with the reported multiport patch antennas supporting at least six radiating waves for either MIMO access points or mobile devices, Table 1 shows a comparison of the proposed eight-port eight-wave antenna (this work in

the table) with the reported six-port six-wave single-patch antennas for access points [19], [20] and for mobile devices [18]. The six-port patch antennas in [19] and [20] require a very high profile of 0.25λ or 0.14λ with respect to the lower-edge frequency of their respective operating band.

On the other hand, the six-port patch antenna in [18] has a low profile of 0.027λ to be suitable for mobile device applications. The proposed eight-port patch antenna also has a comparable low profile of 0.028λ and about 20% in operating bandwidth (about 5.9-7.2 GHz), similar as those in [18] for the six-port six-wave operation.

Note that since these antennas have wide operating bands and the antenna size is generally related to the lowest operating frequency, the corresponding antenna height, patch size, and resonant area for each port are referred to the wavelength of the lowest operating frequency. Also, the operating bandwidths of the antennas in [19] and [20] are based on -10 dB impedance matching for access-point application, while that in [18] and this work are based on 3:1 VSWR or -6 dB impedance matching for mobile device application. The latter bandwidth definition is generally used for the mobile device antennas for practical application considerations, owing to the very limited space available for accommodating the antennas [7], [8], [9], [10], [21], [22].

For the required patch size, the proposed design uses an AR patch of size about $0.64\lambda^2$ to accommodate eight ports. The resonant area for each port (the patch size to port number ratio) is therefore only about $0.080\lambda^2$, which is similar to that ($0.078\lambda^2$) in [18] and much smaller than those ($0.135\lambda^2$, $0.097\lambda^2$) in [19] and [20] for the six-port six-wave operation. In addition, since a single proposed antenna can be applied for 8×8 MIMO operation, different from the six-port patch antennas in [18], [19], and [20] and the four-port patch antennas in [7], [8], [9], [10], [11], [12], [13], [14], [15], [16], and [17], the proposed antenna is expected to be more attractive for the 8×8 MIMO mobile device applications.

Also shown in Table 1, the antenna efficiency, envelope correlation coefficient (ECC), and port isolation over the operating band of the proposed antenna with a compact eight-port eight-wave antenna structure are comparable to those in [18] for the mobile device application.

Furthermore, with the attractive features obtained as described above, the proposed design uses a simple probe feed and a dual-shorting technique for each 45°-ring sector in the AR patch antenna. This leads to a simplified antenna structure as compared to those in [18] based on using a gap-coupled probe feed and a triple-shorting technique for each 60°-disk sector in the six-port circular patch antenna. Detailed antenna structure and performance including the operating principle, parametric study, and experimental results for the eight-port eight-wave AR patch antenna are presented in this study.

II. EIGHT-PORT EIGHT-WAVE AR PATCH NTENNA

Fig. 1 shows the geometry of the wideband low-profile eight-port (Ports 1-8) eight-wave AR patch antenna covering

TABLE 1. Comparison of the six-port six-wave and eight-port eight-wave single-patch antennas for MIMO access points or mobile devices.

Ref.	[19]	[20]	[18]	This work
Number of Ports	Six ports for six waves			Eight ports for eight waves
Operating bandwidth	[a]6.0-8.5 GHz (35%)	[a]3.1-7.2 GHz (80%)	[b]5.8-7.5 GHz (25%)	[b]5.9-7.2 GHz (20%)
Antenna height	High profile, 12.5 mm (0.25λ@6.0GHz)	High profile, 14.0 mm (0.14λ@3.1GHz)	Low profile, 1.4 mm (0.027λ@5.8GHz)	Low profile, 1.4 mm (0.028λ@5.9GHz)
For mobile devices	No, the high profile is suitable for access points		Yes, the low profile is suitable for mobile devices	
Patch shape; Antenna size	Square patch, side edge 45 mm; Size $0.81\lambda^2$ @6.0GHz	Circular patch, diameter 83 mm with the feed; Size $0.58\lambda^2$@3.1GHz	Circular patch, diameter 40 mm; Size $0.47\lambda^2$@5.8GHz	Annular-ring patch, outer diameter 46 mm; Size $0.64\lambda^2$@5.9GHz
Resonant area for each port	$0.135\lambda^2$@6.0GHz	$0.097\lambda^2$@3.1GHz	$0.078\lambda^2$@5.8GHz	$0.080\lambda^2$@5.9GHz
Antenna efficiency	44%-64% for Ports 1-6 at 7.25 GHz	> 85% for Ports 1-6 over the band	50%-62% for Ports 1-6 over the band	46%-62% for Ports 1-8 over the band
ECC	< 0.05	< 0.01	< 0.02	Adjacent ports < 0.08 Other two ports < 0.04
Port isolation	> 20 dB	> 20 dB	Adjacent ports > 10 dB Other two ports > 15 dB	Adjacent ports > 10 dB Other two ports > 21 dB
External feed network	Required, multi-layer technology applied	No	No	No

Note:
a) Operating bandwidth based on -10 dB impedance matching for access-point applications
b) Operating bandwidth based on 3:1 VSWR (-6 dB) for mobile-device applications

5.9-7.2 GHz for 8 × 8 MIMO mobile device applications. The top and side views are shown in Fig. 1(a), while the exploded view is shown in Fig. 1(b). The AR patch has an outer diameter of 46 mm (about 0.91λ at 5.9 GHz) and an inner diameter 11 mm (about 0.24 times the outer diameter). The AR patch is printed on a 0.4 mm thick FR4 substrate of relative permittivity 4.4 and loss tangent 0.02, which is mounted 1.0 mm above a circular ground plane of diameter 55 mm. The total antenna height is therefore 1.4 mm or about 0.028λ at 5.9 GHz.

Note that the effective relative permittivity of the two-layer antenna substrate including the 1.0 mm thick air layer and the 0.4 mm thick FR4 substrate supporting the printed AR patch is about 1.28 only. With the relative permittivity as low as possible, especially close to unity, it has been reported that the bandwidth of the quarterwave patches can be wider than the halfwave patches [23]. This interesting feature is applied in the proposed design to achieve a wide operating band formed by exciting the 0.5- and 0.25-wavelength modes at close frequencies for each port.

In addition, although the lower relative permittivity leads to an increased halfwave patch size, the required AR patch size for eight ports is about $0.64\lambda^2$ at 5.9 GHz and the resonant area for each port is about $0.080\lambda^2$ at 5.9 GHz only. The latter is about the same as that for the low-profile six-port six-wave antenna [18] (see Table 1).

In order to obtain eight isolated resonant patch areas, four open slots of length 46 mm and width 2 mm are embedded in the AR patch to create eight 45°-ring sectors [denoted as Sectors ① -⑧ in Fig. 1(b)] to radiate eight waves. For each ring sector as a halfwave patch, a simple probe feed is placed at the feed circle of radius 17.7 mm and along the centerline of each ring sector to excite the 0.5-wavelength mode. Two shorting pins are then loaded along the shorting circle of radius 15 mm to excite an additional 0.25-wavelength mode of each ring sector as a quarterwave patch.

Note that the shorting circle is at about the electric field null of the 0.5-wavelength mode excited in each ring sector. Therefore, the two shorting pins or the dual-shorting has small effects on the 0.5-wavelength mode. On the other hand, the 0.25-wavelength mode will occur at frequencies close to the 0.5-wavelength mode, mainly owing to the dual-shorting causing a decreased effective resonant length for the quarterwave ring sector. A wideband operation for each port can therefore be formed by the 0.5- and 0.25-wavelength modes.

All the 8 probe feeds and 16 shorting pins in the proposed antenna use a circular copper conductor of diameter 1.6 mm and length 1.4 mm. Note that the two shorting pins are located close to nearby open slots with a short distance (1.8 mm here), so that the excited surface currents coupled into adjacent ring sectors are suppressed. This can increase the port isolation between two adjacent ring sectors. Also, the port isolation of
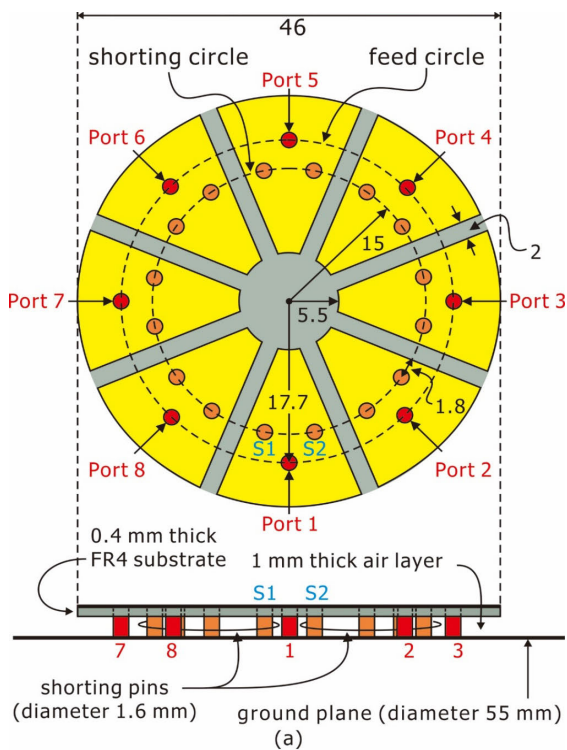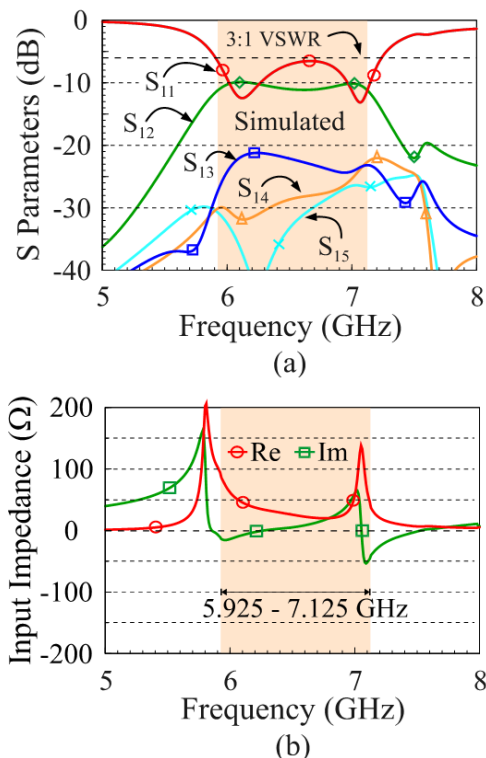
FIGURE 1. Geometry of the wideband low-profile eight-port eight-wave annular-ring patch antenna for 8 × 8 MIMO mobile devices. (a) Top and side views. (b) Exploded view.

FIGURE 2. Simulated (a) S parameters and (b) input impedance of Port 1 in the proposed antenna.

bandwidth 20%), covering the desired 5.925-7.125 GHz (the colored frequency region in the figure) for mobile device applications. The wide operating band is formed by two resonant modes excited at about 6.1 and 7.1 GHz, at which the input reactance (Im) of Port 1 shows about zero reactance as seen in Fig. 2(b).

Also, over the operating band, the transmission coefficient S_{12} (= S_{18}) of Port 1 to adjacent two ports (Ports 2 and 8) is less than −10 dB. Those of Port 1 to other ports (Ports 3-7) are even less than −21 dB [see the curves of S_{13} (= S_{17}), S_{14} (= S_{16}), S_{15}].

It is worthy to note that, the device MIMO with 4Tx/8+Rx is environed for the mobile device in future mobile communications [1]. That is, for the receiving case, Ports 1-8 of the proposed antenna are used. However, for the transmitting case, not all eight ports will be used. Only four ports of the proposed antenna to tarnsmitting 4 MIMO streams are needed. With very high isolation of other two ports (non-adjacent ports) of the proposed antenna obtained, one can use Ports 1, 3, 5, and 7 to transmit 4 MIMO streams in practical applications.

The corresponding simulated vector surface current distributions of Port 1 at the two resonant frequencies are shown in Fig. 3. Also, the simulated electric field distributions in the plane 0.7 mm above the ground plane (in the median plane between the top patch and ground plane) are also plotted in Fig. 4. At 7.1 GHz, the surface currents excited by Port 1 are mainly resonant along the radial direction of Sector ①, and the
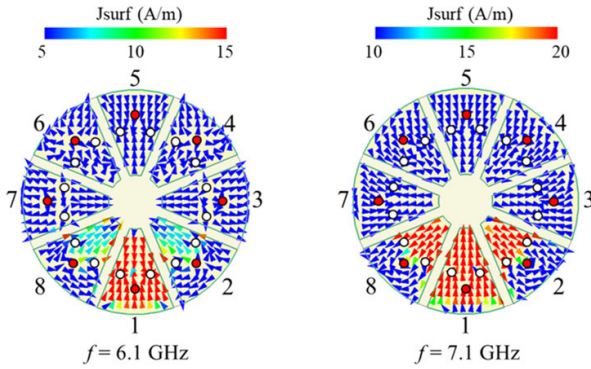
other two ports spaced by one or more ring sectors can be enhanced as well.

The simulated *S* parameters and input impedance of Port 1 in the proposed antenna are shown in Fig. 2. Because of the symmetric structure of the proposed design, the corresponding results of Ports 2-8 are same as that of Port 1. The simulation study is based on applying the commercially available tool of three-dimensional high frequency electromagnetic simulation structure (HFSS) [24].

In Fig. 2(a), the S_{11} is seen to be less than −6 dB or 3:1 VSWR [7], [8], [9], [10] in about 5.9-7.2 GHz (fractional

FIGURE 3. Simulated vector surface current distributions at 6.1 GHz and 7.1 GHz of Port 1 excited with Ports 2-8 terminated to 50 ohms.

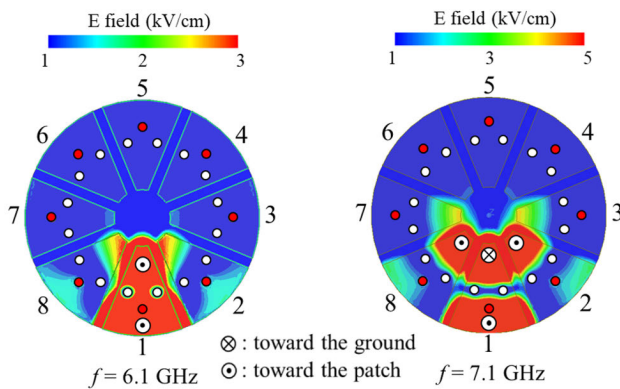**FIGURE 4.** Simulated electric field distributions at 6.1 GHz and 7.1 GHz in the median plane between the top patch and ground plane.

FIGURE 5. Simulated (a) antenna efficiency and antenna gain of Port 1 and (b) envelope correlation coefficients (ECC$_{ij}$) for Ports i and j.

electric fields are directed in different directions (one toward the top patch and one toward the ground plane) on two sides of the shorting circle.

Also note that the radial length of Sector ① is 17.5 mm (outer radius 23 mm, inner radius 5.5 mm), which is about 0.41λ at 7.1 GHz or about 0.47λ by considering the effective relative permittivity of the antenna substrate being 1.28. The excited resonant mode at 7.1 GHz can therefore be identified to be a 0.5λ mode at 7.1 GHz.

On the other hand, the surface currents at 6.1 GHz are resonant from both the outer and inner edges to the two shorting pins in Sector ①. Yet, the surface currents are of the same phase across Sector ①. The electric fields are also of the same phase on two sides of the shorting circle [see Fig. 4(a)]. Based on the surface current and electric field characteristics, the excited resonant mode at 6.1 GHz is considered to be a 0.25λ mode.

As for the radial length of Sector ① being about 0.36λ at 6.1 GHz, relatively much larger than 0.25λ, it is largely resulted from the dual-shorting which decreases the equivalent resonant length from both the outer and inner edges to the shorting pin position as compared to the single-shorting case. This makes the 0.25λ mode to occur at a higher frequency. In the proposed design, the 0.25λ mode is excited at close
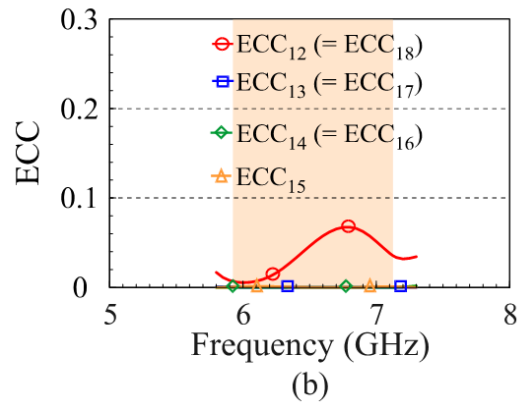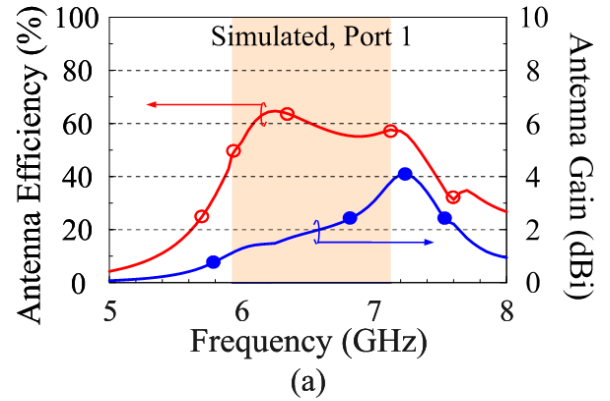
frequencies to the 0.5λ mode, making it possible to form a wide operating band.

Additionally, for Port 1 excited in Sector ①, it is seen that the surface currents coupled to adjacent Sectors ② and ⑧) are generally confined inside the shorting circle. Similar behavior is seen for the electric fields shown in Fig. 4. This suggests that the shorting circle formed by 16 shorting pins seems to function like a circular metal wall in the AR patch. This is expected to increase the port isolation, especially for two adjacent ports, in the proposed antenna.

The simulated radiation characteristics are also studied. In Fig. 5(a), the simulated antenna efficiency and antenna gain are, respectively, about 48%-64% and 1.2-4.1 dBi in 5.925-7.125 GHz (colored frequency region). The results are obtained by considering the impedance matching condition. For the envelope correlation coefficients (ECC$_{ij}$) of Ports i and j shown in Fig. 5(b), they are obtained by using the simulated three-dimensional radiation patterns [25], [26]. Very low ECCs for any two waves radiated by Ports 1-8 are seen. The ECC$_{12}$ (= ECC$_{18}$) for two adjacent ports is less than 0.07, while those for other two ports are less than 0.01. Although the eight ring sectors with Ports 1-8 are very close to each other, the eight radiated waves have very low correlation or can be considered to be uncorrelated, which is promising for 8 × 8 MIMO operation.

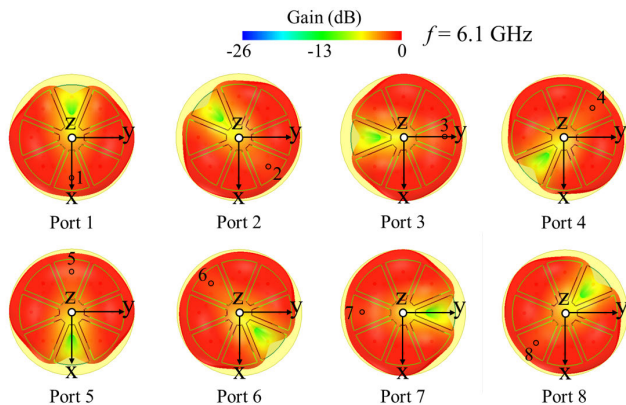**FIGURE 6.** Simulated three-dimensional total-power radiation patterns seen from the *z* direction of Ports 1-8 at 6.1 GHz.
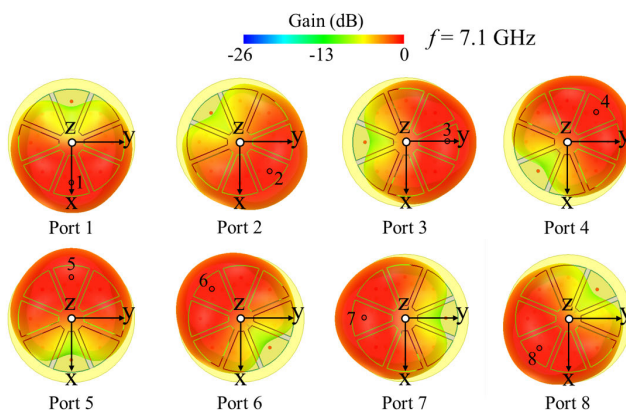

FIGURE 7. Simulated three-dimensional total-power radiation patterns seen from the *z* direction of Ports 1-8 at 7.1 GHz.

To further analyze the radiation patterns of the eight waves, Figs. 6 and 7 show the simulated three-dimensional total-power radiation patterns seen from the *z* direction of Ports 1-8 at 6.1 and 7.1 GHz. For each port, its corresponding radiation pattern is seen to cover a wide area in the azimuthal direction, especially at 6.1 GHz. This behavior is considered to be advantageous for better reception of the incoming line-of-sight and multipath signals from various directions for each port in the proposed 8-port antenna. This attractive wide-pattern feature for each port and the low ECCs for Ports 1-8 are expected to exhibit good 8 × 8 MIMO operation.

III. OPERATING PRINCIPLE
To address in more detail the operating principle of the proposed 8-port antenna, the geometries of the case without shorting pins in each ring sector (denoted as Case A) and the case with one shorting pin along the centerline of each ring sector (denoted as Case B) shown in Fig. 8 are studied. Other corresponding dimensions of Cases A and B are same as the proposed antenna in Fig. 1.

Their simulated *S* parameters of Port 1 are presented in Fig. 9. Only one resonant mode excited at about 6.8 GHz is seen for Case A in Fig. 9(a), which is similar to the 0.5λ
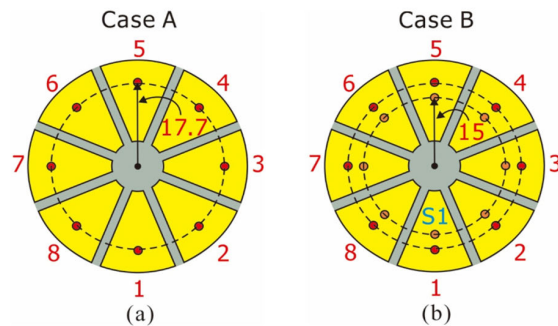

FIGURE 8. Geometries of (a) the case without shorting pins in each ring sector (Case A) and (b) the case with one shorting pin along the centerline of each ring sector (Case B). Other corresponding dimensions are same as the proposed antenna in Fig. 1.
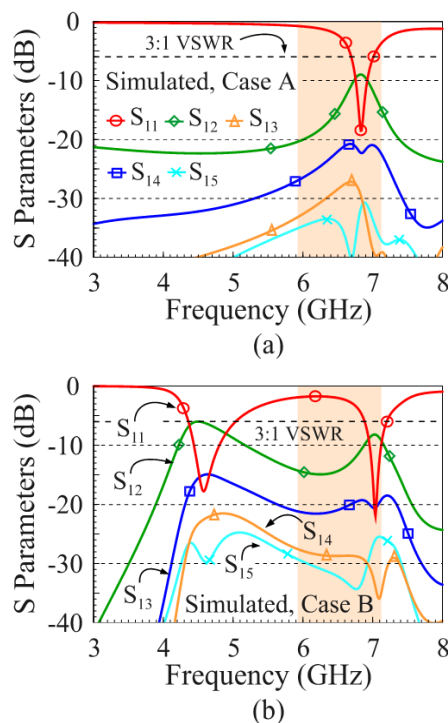

FIGURE 9. Simulated S parameters of Port 1. (a) Case A. (b) Case B.

mode occurred at about 7.1 GHz in the proposed antenna. From the simulated vector surface currents and electric field distributions for Case A shown in Fig. 10, the resonant mode at 6.8 GHz can be identified as a 0.5λ mode.

Note that the feed in each sector is located in the radial direction and the excited surface currents at 6.8 GHz for the first resonance are seen to resonate in the radial direction [see Fig. 10(a)]. Therefore, it can be excepted that the resonant frequency of the first resonance is related to the radial length of each sector. With the outer radius (R_{out}) and inner radius (R_{in}) of each sector to be 23 mm and 5.5 mm (see Fig. 1), respectively, the radial length of each sector is 23 mm − 5.5 mm = 17.5 mm. In this case, the resonant frequency of the first
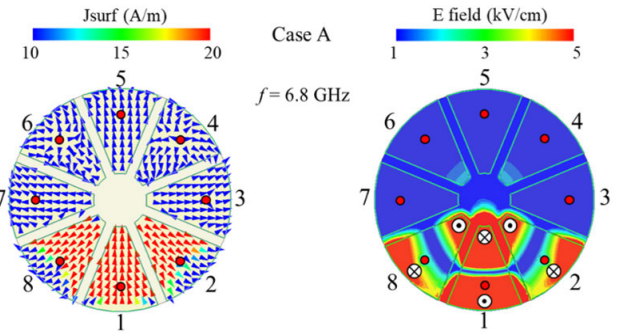
FIGURE 10. Simulated (a) vector surface current distributions on the ring patch and (b) electric field distributions in the median plane between the top patch and ground plane for Port 1 excited at 6.8 GHz in Case A; Other ports are terminated to 50 ohms.

resonance (0.5λ mode) can be estimated by

$$f_1 \cong c/[2(\varepsilon_{\text{eff}})^{1/2}(R_{\text{out}} - R_{\text{in}})] \qquad (1)$$

In Eq. (1), c is the speed of light, ε_{eff} is the effective relative permittivity (1.28 here) of the antenna substrate, and $R_{\text{out}} - R_{\text{in}}$ is the radial length of each sector. From Eq. (1), f_1 is calculated to be about 7.6 GHz, which is about 1.12 times 6.8 GHz observed in Fig. 9(a). The deviation may be owing to the effects of the non-uniform width of each sector and the compact integration of the 8 sectors in the proposed antenna.

In Case B with one shorting pin, an additional 0.25λ mode is excited at about 4.6 GHz and the 0.5λ mode is slightly shifted from 6.8 GHz to occur at 7.0 GHz. The two modes are excited at frequencies far apart, thus they are not able to be combined into a wide operating band.

In addition, the transmission coefficient S_{12} reaches about −5 dB at frequencies where the 0.25λ mode is excited, indicating low port isolation or high port coupling. Similarly, the S_{12} is also about −8 dB at 7.0 GHz where the 0.5λ mode occurs. This agrees with the results shown in Fig. 11, in which the vector surface current and electric field distributions in two adjacent sectors of Sector ① with Port 1 excitation are strong inside and outside the shorting circle formed by total 8 shorting pins in Case B. This behavior will lead to poor port isolation.

By applying the dual shorting in each ring sector of the proposed antenna, the 0.25λ mode is shifted to occur at close frequencies near the 0.5λ mode for wideband operation. As discussed earlier, this is owing to the decreased effective resonant length of the 0.25λ mode, caused by the dual shorting.

In addition, because of the dual shorting placed along the shorting circle, which is located nearby or at the electric field null of the 0.5λ mode, small effect on the 0.5λ mode is expected. This allows the two resonant modes to be combined into a wide operating band.

It is also worth mentioning that, with the dual shorting applied in the proposed antenna, the S_{12} is improved to be less than −10 dB and other transmission coefficients are even less than −20 dB, as shown in Fig. 2. By comparing the results
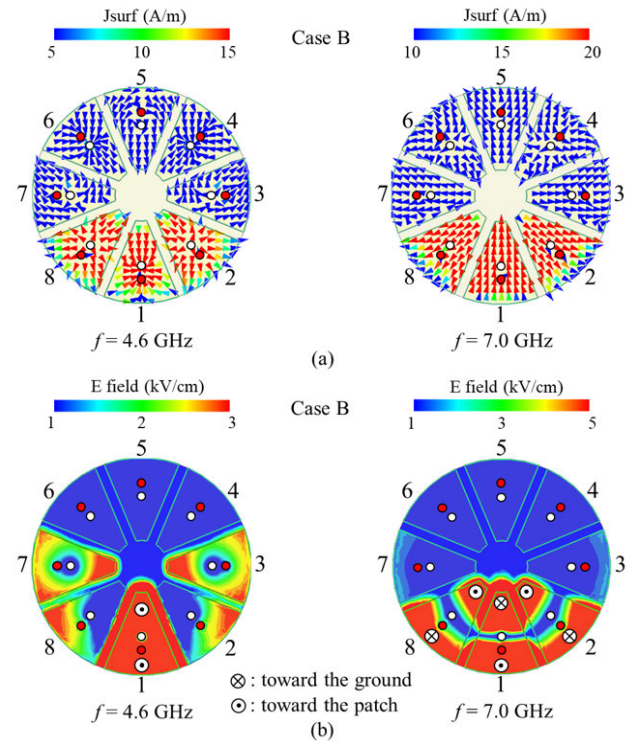

FIGURE 11. Simulated (a) vector surface current distributions on the ring patch and (b) electric field distributions in the median plane between the top patch and ground plane for Port 1 at 4.6 and 7.0 GHz in Case B; Other ports are terminated to 50 ohms.

shown in Figs. 3 and 4 with those in Fig. 11, the surface current and electric field distributions in adjacent sectors of Sector ① are seen to be generally confined inside the shorting circle in the proposed antenna. This can explain the enhanced port isolation obtained in the proposed antenna, owing to the shorting circle formed by the 16 shorting pins of the eight ring sectors therein.

Finally, the annular-ring patch selected to have an outer radius of 23 mm (R_{out}) and an inner radius of 5.5 mm (R_{in}) in the proposed antenna is discussed. By considering that the required resonant area of each port or each radiating element in the reported 6-port circular patch antenna in [18] is about 0.08λ² (λ is the wavelength of the lowest operating frequency of the antenna), the total size of 8 × 0.08λ² = 0.64λ² is therefore selected as the targeted size of the annular-ring patch in the proposed antenna; although when more ports are closely located, larger resonant areas are generally required to achieve good isolation between all radiating elements. This is owing to the increasing coupling between the closely located radiating elements. With the lowest operating frequency at about 5.9 GHz (λ = 50.85 mm), the required outer radius is therefore determined to be about 23 mm [= (0.64λ²/π)^{1/2}].

For the inner radius, it is required in the proposed antenna to achieve a better isolation of Ports 1-8. This is because of the narrow flare angle (45°) of each radiating sector around the patch center in the proposed antenna. This will increase the coupling between the 8 radiating sectors and
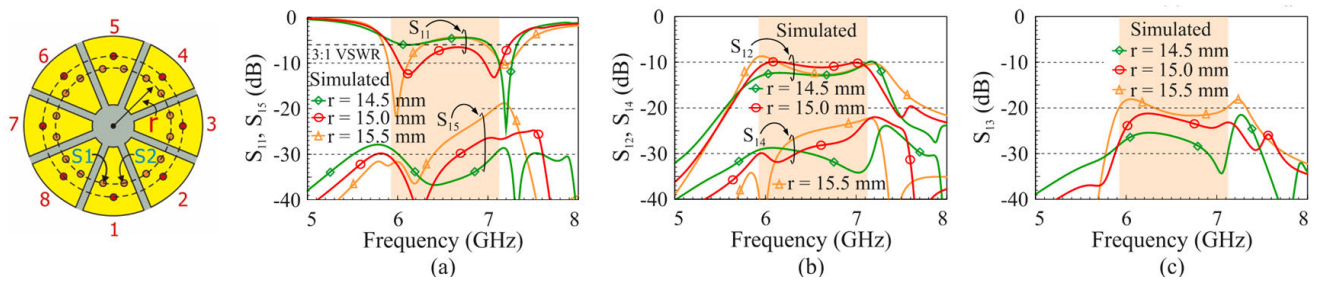
FIGURE 12. Simulated S parameters of Port 1 for the shorting pins at different shorting circles (r). (a) S_{11}, S_{15}. (b) S_{12} (= S_{18}), S_{14} (= S_{18}). (c) S_{13} (= S_{17}). Other antenna parameters are same as in Fig. 1.
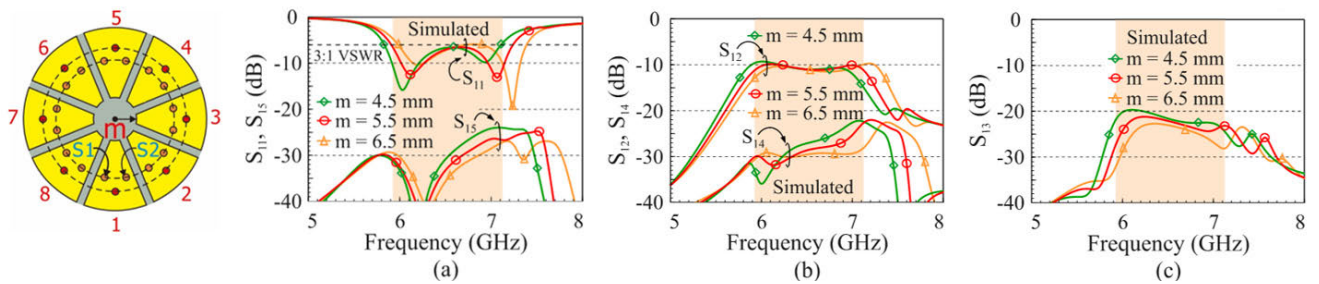
FIGURE 13. Simulated S parameters of Port 1 for various inner AR patch radii (m). (a) S_{11}, S_{15}. (b) S_{12} (= S_{18}), S_{14} (= S_{16}). (c) S_{13} (= S_{17}). Other antenna parameters are same as in Fig. 1.

decrease the port isolation. Detailed results are provided in Fig. 13 for the parametric study of the inner radius effects.

It is also noted that when a larger inner radius is selected, the effective resonant length of each ring sector will be decreased, which increases the resonant frequency of the excited resonant modes. Therefore, based on the parametric study, the inner radius is selected to be 5.5 mm only. In this case, acceptable port isolation is obtained and the outer radius can be kept to be 23 mm to cover the desired 5.9-7.2 GHz band.

IV. PARAMETRIC STUDY
For finely adjusting the design dimensions of the proposed antenna, a parametric study on the shorting circle radius, inner AR patch radius, and feed position is conducted. Fig. 12 shows the simulated S parameters of Port 1 for the shorting pins at different shorting circle radii (r) of 14.5, 15.0, 15.5 mm. Other antenna dimensions are fixed as in Fig. 1. Results of the S_{11} and S_{15} are shown in Fig. 12(a), those of the S_{12} (= S_{18}) and S_{14} (= S_{16}) are in Fig. 12(b), and those of the S_{13} (= S_{17}) are in Fig. 12(c).

When the shorting circle radius is larger (that is, closer to the feed position), relatively large effects on the excitation of the 0.25λ and 0.5λ modes are seen. The transmission coefficients are also increased, indicating that the port isolation is degraded. On the other hand, when the shorting circle radius is smaller, the 0.25λ mode at about 6.1 GHz cannot be excited with good impedance matching. Therefore, the shorting circle radius can be finely adjusted to achieve better impedance matching and port isolation over the desired wide band for the proposed antenna.
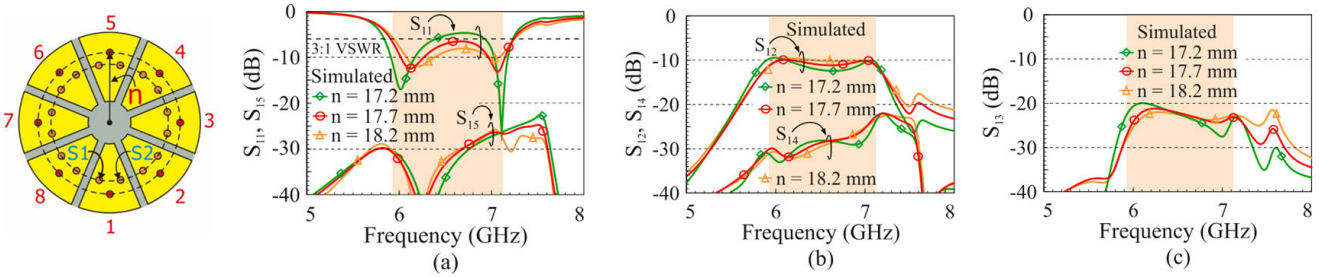
Fig. 13 shows the simulated S parameters of Port 1 for the inner AR patch radius (m) varied from 4.5 to 6.5 mm. Since the variation in the radius m will affect the effective resonant length of each ring sector, the resonant frequencies of the 0.25λ and 0.5λ modes are both varied [see Fig. 13(a)]. The impedance matching of the 0.25λ and 0.5λ modes, however, is not so strongly affected as seen in Fig. 12(a) for the shorting circle radius variation. This can be applied to finely adjust the occurrence of the desired 0.25λ and 0.5λ modes to cover the operating band of interest.

Also note that the S_{12} (= S_{18}) of two adjacent ports are increased with a smaller radius m [see Fig. 13(b)]. This is mainly owing to the narrow flare angle (45°) of each ring sector around the patch center for the proposed 8-port antenna. Therefore, by selecting a proper radius m, it is also helpful to achieve the port isolation to be better than 10 dB for two adjacent ports. While for other two ports, their isolation is still better than 20 dB as seen in the figure.
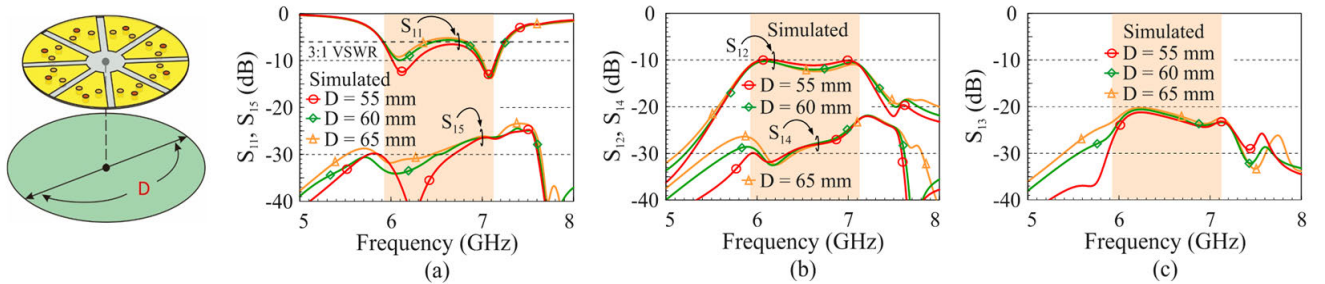
Fig. 14 shows the simulated S parameters of Port 1 for different feed positions (n). Effects on the resonant frequency of the first mode (0.25λ mode) are seen to be larger than that of the second mode (0.5λ mode) [see Fig. 14(a)]. On the other hand, effects on the transmission coefficients of any two ports are small. This behavior can be applied to finely adjust the occurrence of the 0.25λ mode to combine with the 0.5λ mode, thereby achieving better impedance matching over the desired wide operating band.

Effects of the ground plane size are also analyzed. Fig. 15 shows the simulated S parameters of Port 1 for different ground plane diameters (D). Other parameters are fixed as in Fig. 1. When the ground plane diameter increases, the

FIGURE 14. Simulated S parameters of Port 1 for different feed positions (*n*). (a) S_{11}, S_{15}. (b) S_{12} (= S_{18}), S_{14} (= S_{16}). (c) S_{13} (= S_{17}). Other antenna parameters are same as in Fig. 1.

FIGURE 15. Simulated S parameters of Port 1 for different ground plane diameters (*D*). (a) S_{11}, S_{15}. (b) S_{12} (= S_{18}), S_{14} (= S_{16}). (c) S_{13} (= S_{17}). Other antenna parameters are same as in Fig. 1.

S_{11} for the first mode (0.25λ mode) is slightly degraded [see Fig. 15(a)]. This is largely because the first mode has a larger wavelength over the antenna's operating band, thereby causing relatively larger effects on the ground plane size. In this case, by finely adjusting the antenna parameters, better impedance matching of the first mode can still be obtained. On the other hand, small effects are seen for the transmission coefficients. This indicates that the port isolation is insensitive to the ground size variations.

To demonstrate when the proposed antenna is to be placed on a large metal surface, such as measuring 150 mm x 70 mm for the modern smartphone size, the antenna dimensions can be finely adjusted based on the parametric study here. The shorting circle radius, inner AR patch radius, and feed position are adjusted to be 14.7 mm (*r*), 5.2 mm (*m*), and 18.0 mm (*n*), respectively. With the finely adjusted parameters and other antenna dimensions fixed as in Fig. 1, the corresponding simulated S parameters of Port 1 are shown in Fig. 16. In this case, for the proposed antenna placed on a large metal surface, the obtained S parameters can be similar to those shown in Fig. 2.

V. EXPERIMENTAL RESULTS AND DISCUSSION

The 8-port 8-wave patch antenna was fabricated and experimentally studied to verify the simulation prediction. Fig. 17 shows the top, side, and back views of the fabricated antenna. The measured reflection coefficients of Ports 1-4 and Ports 5-8 are respectively shown in Fig. 18(a) and (b).

The measured transmission coefficients for two adjacent ports [S_{12} or $S_{i(i+1)}$] are presented in Fig. 19(a), and those
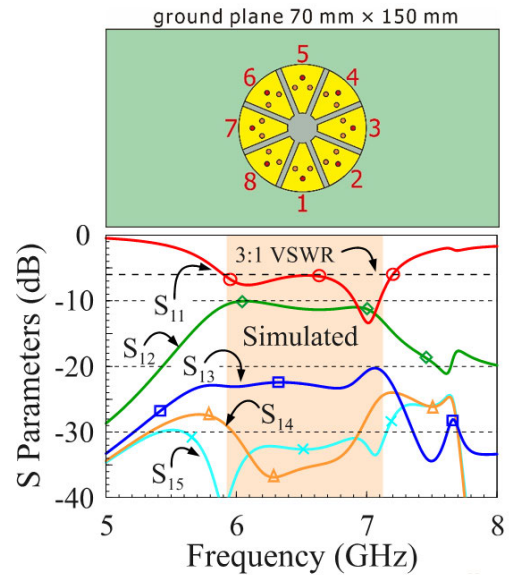
FIGURE 16. Simulated S parameters of Port 1 for the antenna placed on a large metal surface measuring 150 mm × 70 mm, such as the size of the modern smartphone. The shorting circle radius, inner AR patch radius, and feed position of the antenna are finely adjusted.

for two ports spaced by one ring sector [S_{13} or $S_{i(i+2)}$] are in Fig. 19(b). Also, the corresponding measured results for two ports spaced by two ring sectors [S_{14} or $S_{i(i+3)}$] and by three ring sectors [S_{15} or $S_{i(i+4)}$] are respectively shown in Fig. 20(a) and (b). The measured data confirm the simulated results. Ports 1-8 can cover the desired 5.925-7.125 GHz band
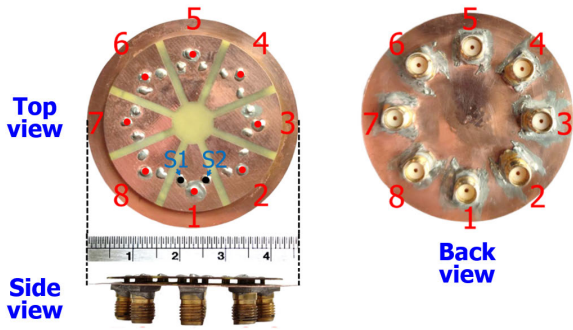
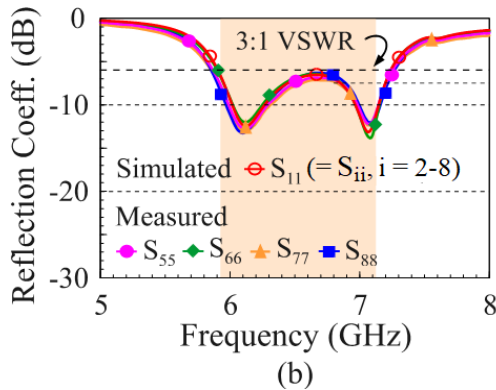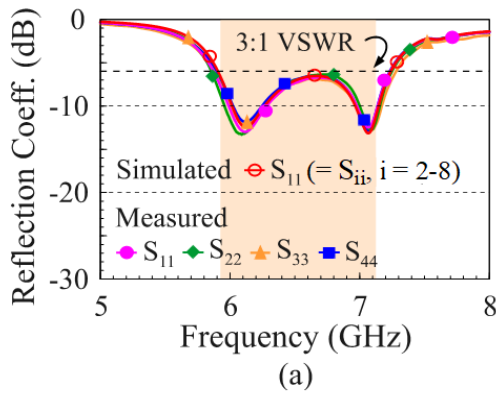**FIGURE 17.** Fabricated eight-port eight-wave patch antenna.

FIGURE 18. Measured reflection coefficients. (a) Ports 1-4. (b) Ports 5-8.

FIGURE 19. Measured transmission coefficients. (a) Two adjacent ports. (b) Two ports spaced by one ring sector.

(the colored frequency region in the figure). The port isolation is better than 10 dB for two adjacent ports and larger than 21 dB for other two ports, which agree with the simulation prediction.

Fig. 21(a) and (b) respectively show the measured antenna efficiency of Ports 1-4 and Ports 5-8. The antenna's radiation performance is measured in a far-field anechoic chamber. Fig. 22 shows the experimental setup snapshot of the fabricated antenna supported by a two-axis positioner to be rotated in the θ and φ directions in the chamber.

Based on the Great circle test method [27], the radiated electric fields over the sphere surrounding the antenna were measured to evaluate the antenna efficiency. Agreement between the measurement and simulation is generally
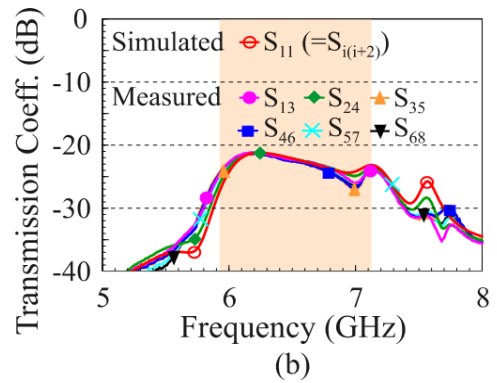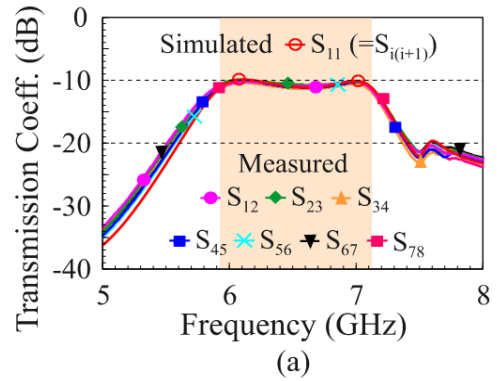
obtained. The measured antenna efficiency is about 46%-62% over the operating band.

By using the measured three-dimensional radiated fields including the amplitude and phase [25], [26], the ECC_{ij} between two ports (Ports i and j) is calculated. Representative calculated ECCs are shown in Fig. 23. Small values of the ECCs of two adjacent ports less than about 0.08 and other two ports less than about 0.04 are obtained. The results generally confirm the simulated ECCs in Fig. 5(b).

Figs. 24 and 25 show the measured and simulated normalized radiation patterns respectively for Ports 1-4 and Ports 5-8 in the plane along the centerline of their corresponding ring sectors. The results at 6.1 GHz for the 0.25λ mode and at 7.1 GHz for the 0.5λ mode are presented.

For Ports 1-8, their corresponding radiation patterns along the $\varphi = 0^{\circ}$ (Port 1), 45° (Port 2), 90° (Port 3), 135° (Port 4), 180° (Port 5), 225° (Port 6), 270° (Port 7), and 315° (Port 8) planes are plotted. Note that the simulated E_{φ} component is very small $(< -40\,\text{dB})$ along the centerline of each ring sector and is thus not shown in the figure. Generally, the measured and simulated radiation patterns are in agreement.

It is also observed that the radiation pattern of each port is tilted away from the patch center and toward the feed direction. This is related to more surface currents being excited near the outer edge of each ring sector. This behavior is considered to be helpful for achieving low ECC values of the eight waves generated by the proposed antenna.
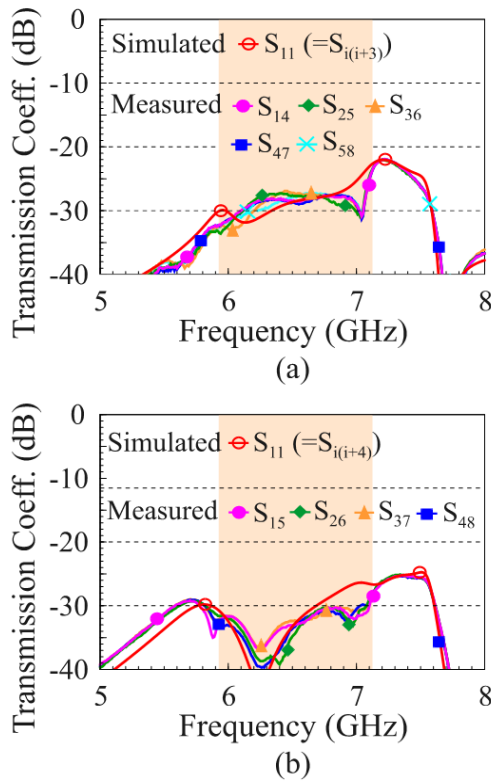
FIGURE 20. Measured transmission coefficients. (a) Two ports spaced by two ring sectors. (b) Two ports spaced by three ring sectors.
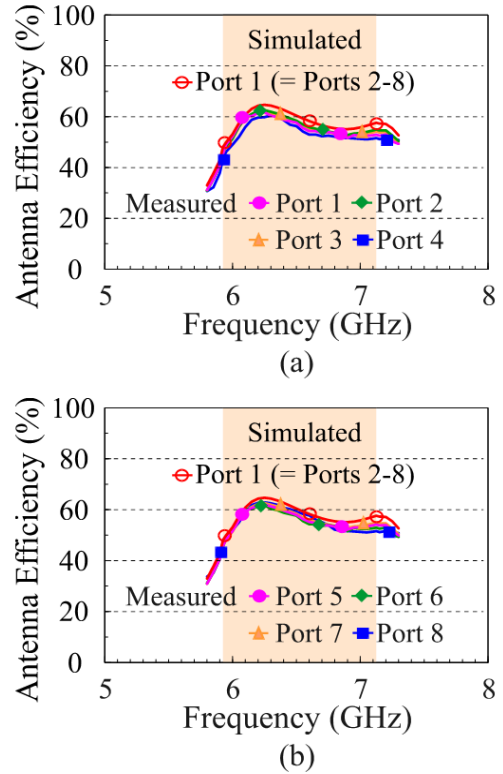

FIGURE 21. Measured antenna efficiency. (a) Ports 1-4. (b) Ports 5-8.

VI. 8 × 8 MIMO TESTING OF THE PROPOSED ANTENNA

To test the proposed 8-port patch antenna for the 8 × 8 MIMO operation, the antenna shown in Fig. 16 integrated with a ground plane of size 150 mm × 70 mm (typical modern smartphone size) was fabricated and tested in our 8 × 8 MIMO testbed developed in NSYSU [2] as shown in Fig. 26. The testing frequency band is selected to be 7025-7125 MHz with 100 MHz bandwidth within the operating bandwidth of the proposed antenna. In 2019 World Radiocommunication Conference (WRC-19), this frequency band has been agreed to be considered as a new possible mobile communication spectrum globally and will be decided in 2023 World Radiocommunication Conference (WRC-23) [4].

At the transmitter (Tx) side, two 4-port antennas (total size 150 mm × 70 mm) based on the 4-port patch antenna reported in [16] are fabricated. The two 4-port antennas are designed to cover the testing frequency band and used to transmit 8 MIMO signals in the MIMO testing. All eight ports in the two 4-port antennas are connected to eight RF vector signal generators SGT100A with an integrated baseband generator [28].

On the other hand, at the receiver (Rx) side, Ports 1-8 of the proposed 8-port antenna are connected to two 4-port digital oscilloscope RTP084 [28]. The received MIMO signals of Ports 1-8 are finally fed into a desktop computer loaded with
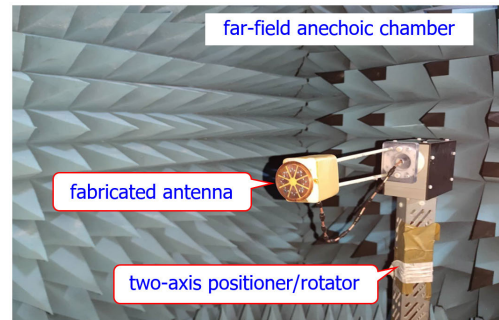

FIGURE 22. Experimental setup of the fabricated antenna tested in the far-field anechoic chamber.
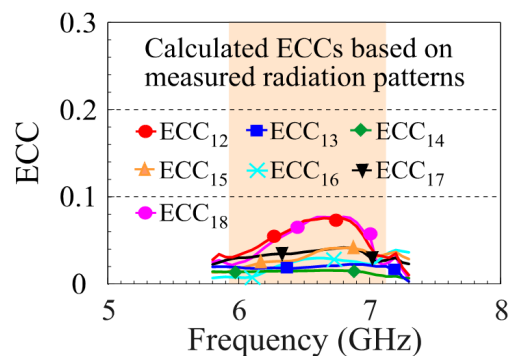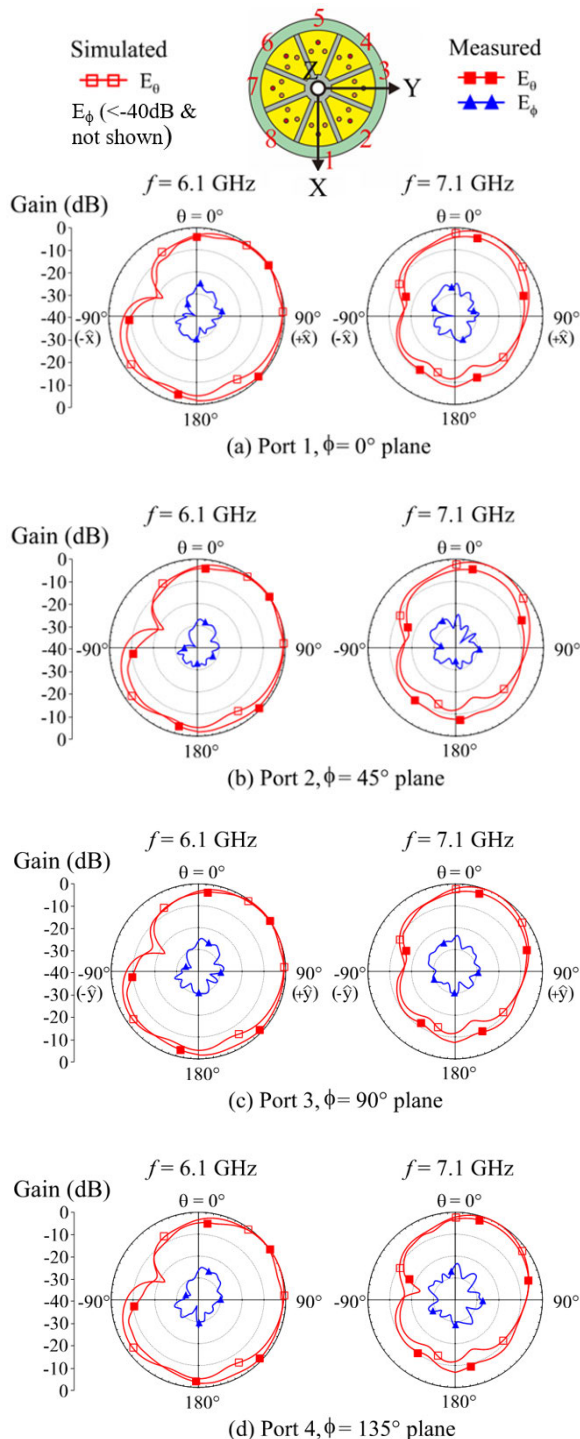

FIGURE 23. Calculated ECCs as a function of the measured three-dimensional radiated fields of the antenna.

the in-house developed software MIMO receiver to obtain the 8 × 8 MIMO capacity and throughout [2].

FIGURE 24. Measured and simulated normalized radiation patterns at 6.1 and 7.1 GHz for Ports 1-4 in the plane along the centerline of their corresponding ring sectors. (a) Port 1. (b) Port 2. (c) Port 3. (d) Port 4.
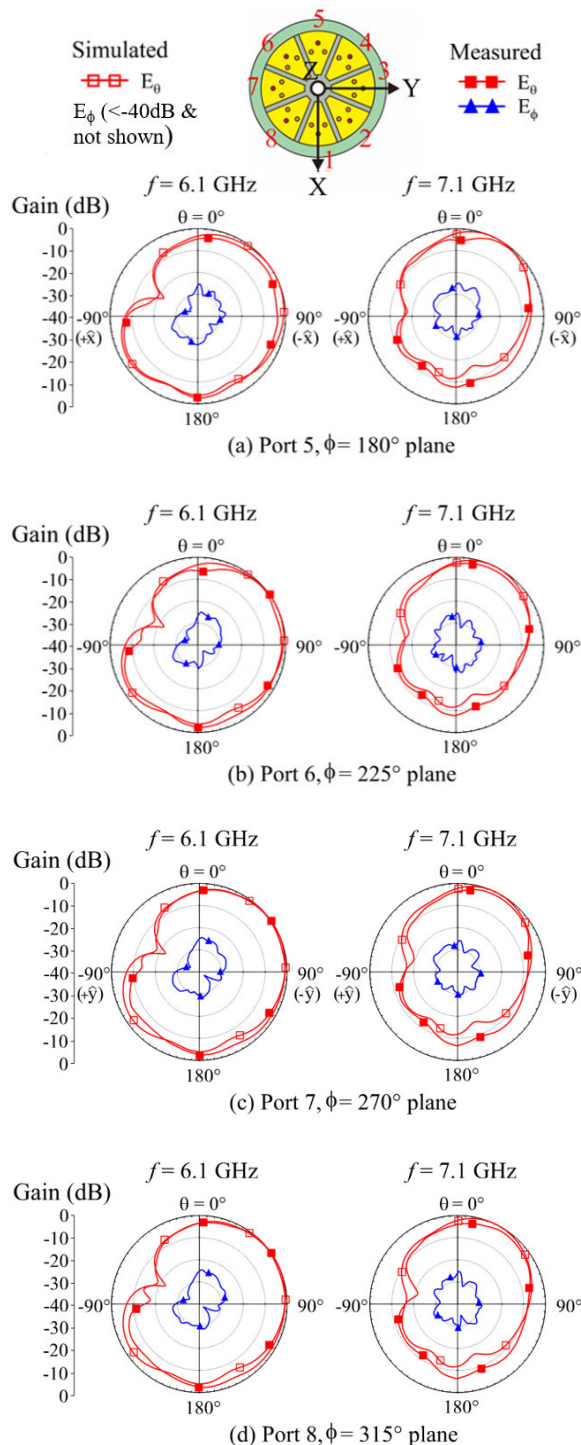
FIGURE 25. Measured and simulated normalized radiation patterns at 6.1 and 7.1 GHz for Ports 5-8 in the plane along the centerline of their corresponding ring sectors. (a) Port 5. (b) Port 6. (c) Port 7. (d) Port 8.

Fig. 27 shows the 8 × 8 MIMO testing scenario in the open space in front of the entrance of the electrical engineering department building, NSYSU. The distance between the Tx and Rx antennas is 9 meters. The measured results are shown in Table 2. The measured signal noise ratios (SNR) of

Ports 1-8 of the Rx antenna (the proposed antenna in Fig. 16) are provided. The average SNR of the received eight signals is about 26.4 dB. Variations of the received SNRs of the eight ports are related to the complex multipath scattering in the practical MIMO propagation scenario.
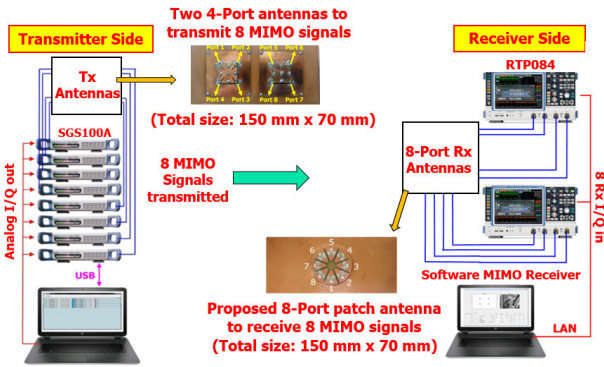
FIGURE 26. Schematic diagram of the 8 × 8 MIMO testbed developed in National Sun Yat-sen University (NSYSU) [2]. Rx antennas are the fabricated 8-port antenna in Fig. 16. Tx antennas uses two 4-port antennas studied in [16] to transmit 8 MIMO signals.
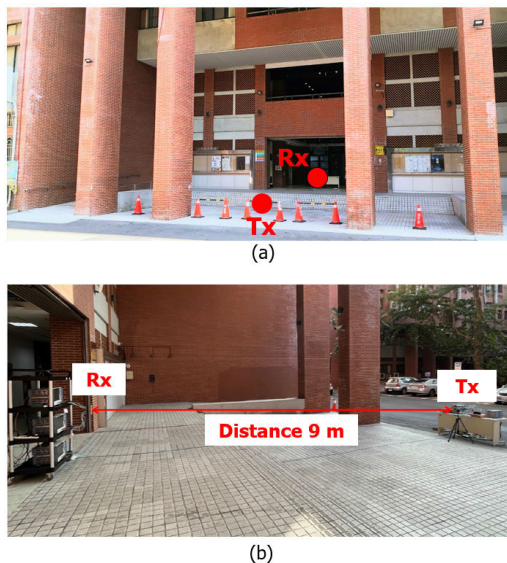
FIGURE 27. (a) The 8 × 8 MIMO testing in the open space in front of the entrance of the EE department building, NSYSU. (b) Tx and Rx distance is 9 meters. The proposed antenna is used as the receive antennas at Rx side.

The measured MIMO capacity is 42.8 bps/Hz, which suggests that the 8 × 8 MIMO operation in this study with 100 MHz bandwidth can ideally support a data throughput up to 4.28 Gbps. However, the practical data throughput generally cannot reach the ideal value.

In this study, based on using the 64-QAM (Quadratic Amplitude Modulation) signal modulation, the measured 8 × 8 MIMO throughput is 3476 Mbps, which is the correct data received at the Rx side. The uncoded bit error rate (BER) is 0.013 only. Note that, with the uncoded BER less than 0.1, it can generally be corrected to obtain a zero BER [2] in practical communications. That is, the proposed 8-port antenna applied in the 8 × 8 MIMO testing can support the 64-QAM modulation. The corresponding spectral efficiency is then evaluated to be 34.76 bps/Hz (total throughput divided by the 100 MHz bandwidth).

TABLE 2. Measured 8 × 8 MIMO capacity/throughput of the proposed antenna in Fig. 16. The MIMO testbed and testing scenario are shown in Figs. 26 and 27.

f_0 = 7075 MHz (7025-7125 MHz, 100 MHz bandwidth), 8 × 8 MIMO, Signal Modulation: 64 QAM	
Transmit antennas (Two 4-Port patch antennas [16] to transmit 8 MIMO signals)	Receive antennas (Proposed 8-Port patch antenna to receive 8 MIMO signals)
Measured Signal Noise Ratio (dB)	26.4, 25.4, 26.3, 26.7, 26.8, 25.8, 27.7, 25.9 (Ports 1-8)
Measured 8 x 8 MIMO Capacity	42.8 bps/Hz
Uncoded Bit Error Rate	0.013
Measured 8 x 8 MIMO Throughput	3476 Mbps
8 x 8 MIMO Spectral Efficiency	34.76 bps/Hz

Also note that, the obtained 4 × 4 MIMO throughput with 100 MHz bandwidth (5750-5850 MHz) tested in [12] is about 1.6 Gbps only. In the study here, the 8 × 8 MIMO throughput with the proposed 8-port antenna as the Rx antennas can successfully achieve much higher throughput than that of the 4 × 4 MIMO operation. This suggests that the proposed 8-port antenna is promising for the future 8 × 8 MIMO mobile device application to achieve much higher data throughputs.

VII. CONCLUSION

For 8 × 8 MIMO application in the mobile device, a wideband eight-port eight-wave annular-ring patch antenna covering the 6 GHz band (5.925-7.125 GHz) for the possible new mobile frequency spectrum in the future 6G communication system [3], [4] has been presented. The proposed antenna has a low profile of 1.4 mm (about 0.028λ at 5.9 GHz) and an outer diameter of 46 mm (about 0.91λ at 5.9 GHz) to generate eight very-low-correlated waves over the desired wide band with low ECCs. The antenna structure, operating principle, parametric study, and experimental results for the proposed antenna have been addressed. The dual-shorting dual-resonant technique has been successfully applied in the eight 45°-ring sectors in the proposed antenna to achieve both wideband operation and enhanced port isolation. In addition to the 8 × 8 MIMO mobile device application, the proposed antenna will also be promising for the IoT device application for 8 × 8 MIMO operation.

REFERENCES

[1] (Jan. 7, 2022). *MediaTek 6G Vision Whitepaper.* [Online]. Available: https://www.mediatek.com/whitepapers/6g

[2] K.-L. Wong, "5G/B5G multi-Gbps antennas for user terminals and their throughput verification," in *Proc. IEEE Asia–Pacific Microw. Conf. (APMC)*, Hong Kong, Dec. 2020, pp. 366–368.

[3] (Nov. 1, 2021). *6G: The Next Horizon, Huawei 6G Research Team.* [Online]. Available: https://www.huawei.com/en/technology-insights/future-technologies/6g-the-next-horizon

[4] (Nov. 6, 2019). *WRC-19 (World Radiocommunication Conference 2019) Report. Key Outcomes of the WRC-19.* [Online]. Available: https://www.itu.int/en/itunews/Documents/2019/2019-06/2019_ITUNews06-en.pdf

[5] (Apr. 2, 2020). *Unlicensed Use of the 6 GHz Band, Federal Communications Commission Fact Sheet*. [Online]. Available: https://docs.fcc.gov/public/attachments/DOC-363490A1.pdf

[6] (May 17, 2022). *2022 Spectrum Development, National Spectrum Development Association*. [Online]. Available: https://www.nsma.org/wp-content/uploads/9.-State-of-the-Spectrum_Remaley-Conway.pdf

[7] L. Chang and H. Wang, "Miniaturized wideband four-antenna module based on dual-mode PIFA for 5G 4×4 MIMO applications," *IEEE Trans. Antennas Propag.*, vol. 69, no. 9, pp. 5297–5304, Sep. 2021.

[8] L. Chang, G. Zhang, and H. Wang, "Triple-band microstrip patch antenna and its four-antenna module based on half-mode patch for 5G 4×4 MIMO operation," *IEEE Trans. Antennas Propag.*, vol. 70, no. 1, pp. 67–74, Jan. 2022.

[9] I. R. R. Barani, K. L. Wong, Y. X. Zhang, and W. Y. Li, "Low-profile wideband conjoined open-slot antennas fed by grounded coplanar waveguides for 4×4 5G MIMO operation," *IEEE Trans. Antennas Propag.*, vol. 68, pp. 2646–2657, Apr. 2020.

[10] K. L. Wong, M. F. Jian, and W. Y. Li, "Low-profile wideband four-corner-fed square patch antenna for 5G MIMO mobile antenna application," *IEEE Antennas Wireless Propag. Lett.*, vol. 20, no. 12, pp. 2054–2058, Dec. 2021.

[11] H. T. Chattha, M. K. Ishfaq, B. A. Khawaja, A. Sharif, and N. Sheriff, "Compact multiport MIMO antenna system for 5G IoT and cellular handheld applications," *IEEE Antennas Wireless Propag. Lett.*, vol. 20, no. 11, pp. 2136–2140, Nov. 2021.

[12] K.-L. Wong, C.-J. Chen, and W.-Y. Li, "Integrated four low-profile shorted patch dual-band WLAN MIMO antennas for mobile device applications," *IEEE Trans. Antennas Propag.*, vol. 69, no. 6, pp. 3566–3571, Jun. 2021.

[13] W. Su, Q. Zhang, S. Alkaraki, Y. Zhang, X.-Y. Zhang, and Y. Gao, "Radiation energy and mutual coupling evaluation for multimode MIMO antenna based on the theory of characteristic mode," *IEEE Trans. Antennas Propag.*, vol. 67, no. 1, pp. 74–84, Jan. 2019.

[14] N. L. Johannsen, N. Peitzmeier, P. A. Hoeher, and D. Manteuffel, "On the feasibility of multi-mode antennas in UWB and IoT applications below 10 GHz," *IEEE Commun. Mag.*, vol. 58, no. 3, pp. 69–75, Mar. 2020.

[15] K.-L. Wong, J.-Z. Chen, and W.-Y. Li, "Four-port wideband annular-ring patch antenna generating four decoupled waves for 5G multi-input–multi-output access points," *IEEE Trans. Antennas Propag.*, vol. 69, no. 5, pp. 2946–2951, May 2021.

[16] K.-L. Wong, X.-Q. Ye, and W.-Y. Li, "Wideband four-port single-patch antenna based on the quasi-TM$_{1/2,1/2}$ mode for 5G MIMO access-point application," *IEEE Access*, vol. 10, pp. 9232–9240, 2022.

[17] K.-L. Wong, H.-Y. Jiang, and W.-Y. Li, "Decoupling hybrid metal walls and half-wavelength diagonal open-slots based four-port square patch antenna with high port isolation and low radiation correlation for 2.4/5/6 GHz WiFi-6E 4×4 MIMO access points," *IEEE Access*, vol. 10, pp. 81296–81308, 2022.

[18] K.-L. Wong, C.-J. Ho, and W.-Y. Li, "Low-profile six-port circular patch antenna with six triple-shorted dual-resonant 60°-disk sectors to generate six uncorrelated waves for wideband mobile MIMO antennas," *IEEE Access*, vol. 10, pp. 80277–80288, 2022.

[19] N. Peitzmeier, T. Hahn, and D. Manteuffel, "Systematic design of multimode antennas for MIMO applications by leveraging symmetry," *IEEE Trans. Antennas Propag.*, vol. 70, no. 1, pp. 145–155, Jan. 2022.

[20] K.-L. Wong, Z.-W. Tso, and W.-Y. Li, "Very-wide-band six-port single-patch antenna with six uncorrelated waves for MIMO access points," *IEEE Access*, vol. 10, pp. 69555–69567, 2022.

[21] L. Sun, Y. Li, and Z. Zhang, "Wideband integrated quad-element MIMO antennas based on complementary antenna pairs for 5G smartphones," *IEEE Trans. Antennas Propag.*, vol. 69, no. 8, pp. 4466–4474, Aug. 2021.

[22] S.-C. Chen, J.-L. Zhu, and C.-I.-G. Hsu, "Compact double shorted loop sub-6-GHz dual-band MIMO quad-antenna system," *IEEE Access*, vol. 9, pp. 114672–114679, 2021.

[23] K. F. Lee, Y. X. Guo, J. A. Hawkins, R. Chair, and K. M. Luk, "Theory and experiment on microstrip patch antennas with shorting walls," *IEE Proc.-Microw., Antennas Propag.*, vol. 147, no. 6, pp. 521–525, Dec. 2000.

[24] (Mar. 1, 2022). *3D High Frequency Electromagnetic Simulation Software, ANSYS HFSS*. [Online]. Available: https://www.ansys.com/products/electronics/ansys-hfss

[25] A. Iqbal, A. Altaf, M. Abdullah, M. Alibakhshikenari, E. Limiti, and S. Kim, "Modified U-shaped resonator as decoupling structure in MIMO antenna," *Electronics*, vol. 9, no. 8, p. 1321, Aug. 2020.

[26] S. Blanch, J. Romeu, and I. Coebella, "Exact representative of antenna system diversity performance from input parameter description," *Electron. Lett.*, vol. 39, pp. 705–707, May 2003.

[27] Y. Okano and K. Cho, "Antenna measurement system for mobile terminals," *NTT DoCoMo Tech. J.*, vol. 9, no. 2, pp. 43–50, 2007.

[28] Rohde&Schwarz. (Nov. 10, 2022). [Online]. Available: http://www.rohde-schwarz.com.tw/PrecompiledWeb/Index.aspx
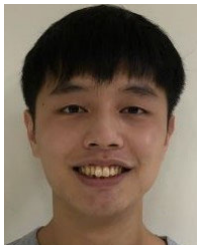
KIN-LU WONG (Fellow, IEEE) received the B.S. degree in electrical engineering from the National Taiwan University, Taipei, Taiwan, in 1981, and the M.S. and Ph.D. degrees in electrical engineering from Texas Tech University, Lubbock, TX, USA, in 1984 and 1986, respectively.

From 1986 to 1987, he was a Visiting Scientist with the Max-Planck-Institute for Plasma Physics, Munich, Germany. Since 1987, he has been with the Electrical Engineering Department, National Sun Yat-sen University (NSYSU), Kaohsiung, Taiwan, where he became a Professor, in 1991. He also served as the Chairperson for the Electrical Engineering Department, from 1994 to 1997, the Vice President for Research Affairs, from 2005 to 2007, and the Senior Vice President at the NSYSU, from 2007 to 2012. From 1998 to 1999, he was a Visiting Scholar with the Electroscience Laboratory, The Ohio State University, Columbus, OH, USA. He was elected to be a Sun Yat-sen Chair Professor at NSYSU, in 2005, a Distinguished Chair Professor at the NSYSU, in 2017, and the National Chair Professor of Ministry of Education of Taiwan, in 2016. He is currently a National Chair Professor of Ministry of Education, a Distinguished Researcher of Ministry of Science and Technology, and a Distinguished Chair Professor with the NSYSU. He has authored more than 580 refereed journal articles and 300 conference papers and has personally supervised 57 graduated Ph.D. He holds over 300 patents, including 103 U.S. patents. He is the author of *Design of Nonplanar Microstrip Antennas and Transmission Lines* (Wiley, 1999), *Compact and Broadband Microstrip Antennas* (Wiley, 2002), and *Planar Antennas for Wireless Communications* (Wiley, 2003). His published articles have been cited over 34,000 times with an H-index of 87 in Google Scholar.

Dr. Wong served or also serves as an IEEE AP-S AdCom Member, an IEEE Transactions on Antennas and Propagation Track Editor/Associate Editor, an IEEE Transactions on Antennas and Propagation Paper Awards Committee Member, and an AP-S Field Awards Committee Member. He received the Outstanding Research Award three times (1995, 2000, and 2002) from the Taiwan National Science Council. He also received the Outstanding Electrical Engineering Professor Award from the Institute of Electrical Engineers of Taiwan, in 2003, and the Outstanding Engineering Professor Award from the Institute of Engineers of Taiwan, in 2004. In 2008, the research achievements on handheld device antennas of NSYSU Antenna Laboratory led by him was selected to be top 50 scientific achievements of the Taiwan Ministry of Science and Technology in past 50 years (1959–2009). He was a recipient of the 2010 Outstanding Research Award of Pan Wen Yuan Foundation and selected as top 100 Honor of Taiwan by Global Views Monthly, in August 2010, for his contribution in mobile antenna researches. He was also a recipient of the Academic Award from the Taiwan Ministry of Education, in 2012, and the Outstanding Distinguished Researcher Award from the Taiwan Ministry of Science and Technology, in 2013. He and his graduate students have been awarded the Best Paper Award (APMC Prize) from 2008 APMC, and the Best Student Paper Award/Young Scientist Award from 2007 ISAP, 2008 APMC, 2009 ISAP, 2010 ISAP, 2012 ISAP, and 2016 ISAP. His graduate students also won the first prize of 2007 and 2009 Taiwan National Mobile Handset Antenna Design Competition. He was awarded the Best Associate Editor two times (2015 and 2016) for the IEEE Transactions on Antennas and Propagation.

He was also a PE7 Panel Member of 2015, 2017, and 2019 European Research Council Advanced Grant Panel, and a Chief Consultant of the Institute of Antenna Engineers of Taiwan. He also served as the Chair for the Judge Panel (2014–2022) of the National Communication Antenna Design Competition organized by the Taiwan Ministry of Economics. He served as the General Chairs for 2012 APMC, 2014 ISAP, and 2016 APCAP held at Kaohsiung, Taiwan. He also serves as the Honorary Chair for 2023 APMC to be held at Taipei, Taiwan. He was elected as a Thomson Reuters Highly Cited Researcher in both 2014 and 2015 and also elected as an Elsevier Most Cited Researcher, in 2015. In 2022, he was selected by Research.com to be ranked #99 in Full World Ranking and #1 in Full Taiwan Ranking in the 2022 Edition of Ranking of Top 1000 Scientists in the field of electronics and electrical engineering. He is a Thomson Reuters Highly Cited Researcher and an Elsevier Most Cited Researcher.

HUI-CHIH KAO (Student Member, IEEE) received the B.S. degree in electrical engineering from the Lunghua University of Science and Technology, Taoyuan City, Taiwan, in 2020. He is currently pursuing the M.S. degree with the National Sun Yat-Sen University, Kaohsiung, Taiwan. His main research interests include multi-port MIMO wideband patch antennas and MIMO capacity/throughput testing for 5G/B5G access-point and mobile-device applications.

WEI-YU LI (Member, IEEE) was born in Taipei, Taiwan, in 1981. He received the B.S. degree in electrical engineering from Feng Chia University, Taichung, Taiwan, in 2004, and the M.S. and Ph.D. degrees in electrical engineering from the National Sun Yat-sen University (NSYSU), Kaohsiung, Taiwan, in 2006 and 2009, respectively.

After graduated from NSYSU, in 2009, he has been with the Information and Communication Research Laboratories (ICL), Industrial Technology Research Institute (ITRI), Hsinchu, Taiwan, participating and leading advanced research for development of emerging wireless antenna technologies. From April to October 2012, he was as an Exchange Guest Researcher with the National Institute of Information and Communications Technology (NICT), Tokyo, Japan. He is currently a Deputy Technology Manager at ITRI. He has authored or coauthored 33 refereed journal articles and 40 conference papers. He holds over 70 patents, including U.S., Taiwan, China, and EU patents. His published articles have been cited over 1,474 times with an H-index of 22 in Google Scholar.

Dr. Li has been selected as an International Steering Committee Member of 2019–2022 ISAP. He also served as an AdCom Member for the Institute of Antenna Engineers of Taiwan (2014, 2015, and 2018–2022). From 2014 to 2022, he also served as a member of the Judge Panel for the National Terminal Antenna Design Competition organized by the Taiwan Ministry of Economics. He received the Young Scientist Award from 2007 ISAP and the Best Paper Award (APMC Prize) from 2008 APMC. He has been a principal investigator or co-principal investigator of many research projects in ITRI and has received numerous recognitions, including the First Prize of the Outstanding Research Award of ITRI, in 2010, the Solar Industrial Award (SIA) of Europe, in 2011, the Outstanding Innovation Award of ITRI, in 2013, the Second Prize of the Outstanding Research Award of ITRI, in 2014, the 2015 Research and Development 100 Award Finalist of the U.S., the Outstanding Innovation Award of ITRI, in 2017, the First Prize of the Outstanding Industrialization Award of ITRI, in 2017, the Second Prize of the Outstanding Industrialization Award of ITRI, in 2020, and the Third Prize of the Outstanding Industrialization Award of ITRI, in 2021. He also received the Outstanding Lecturer Award of ITRI, in 2013, and the International Paper Award of ICL of ITRI, in 2020. He is the Chair of IEEE AP-S Tainan Chapter (2021–2022).

∙ ∙ ∙